Brain Stimulation 12 (2019) 19–29

Contents lists available at ScienceDirect

Brain Stimulation

journal homepage: http://www.journals.elsevier.com/brain-stimulation

Modulation of neuroinflammation and memory dysfunction using percutaneous vagus nerve stimulation in mice

William J. Huffman [a, b, 1], Saraswathi Subramaniyan [b, 1], Ramona M. Rodriguiz [c], William C. Wetsel [c, d], Warren M. Grill [a, e], Niccolò Terrando [b, *]

[a] Department of Biomedical Engineering, Duke University, Durham, NC, 27708, USA
[b] Center for Translational Pain Medicine, Department of Anesthesiology, Duke University Medical Center, Durham, NC, 27710, USA
[c] Department of Psychiatry and Behavioral Sciences, Mouse Behavioral and Neuroendocrine Analysis Core Facility, Duke University Medical Center, Durham, NC, 27710, USA
[d] Department of Neurobiology and Cell Biology, Duke University Medical Center, Durham, NC, 27710, USA
[e] Department of Electrical and Computer Engineering, Neurobiology, and Neurosurgery, Duke University, Durham, NC, 27708, USA

ARTICLE INFO

Article history:
Received 3 April 2018
Received in revised form
2 October 2018
Accepted 3 October 2018
Available online 9 October 2018

Keywords:
Cognition
Cytokines
Microglia
Neuroinflammation
Percutaneous
Vagus nerve stimulation

ABSTRACT

Background: The vagus nerve is involved in regulating immunity and resolving inflammation. Current strategies aimed at modulating neuroinflammation and cognitive decline, in many cases, are limited and ineffective.
Objective: We sought to develop a minimally invasive, targeted, vagus nerve stimulation approach (pVNS), and we tested its efficacy with respect to microglial activation and amelioration of cognitive dysfunction following lipopolysaccharide (LPS) endotoxemia in mice.
Methods: We stimulated the cervical vagus nerve in mice using an ultrasound-guided needle electrode under sevoflurane anesthesia. The concentric bipolar needle electrode was percutaneously placed adjacent to the carotid sheath and stimulation was verified in real-time using bradycardia as a biomarker. Activation of vagal fibers was confirmed with immunostaining in relevant brainstem structures, including the dorsal motor nucleus and nucleus tractus solitarius. Efficacy of pVNS was evaluated following administration of LPS and analyses of changes in inflammation and behavior.
Results: pVNS enabled stimulation of the vagus nerve as demonstrated by changes in bradycardia and histological evaluation of c-Fos and choline acetyltransferase expression in brainstem nuclei. Following LPS administration, pVNS significantly reduced plasma levels of tumor necrosis factor-α at 3 h post-injection. pVNS prevented LPS-induced hippocampal microglial activation as analyzed by changes in Iba-1 immunoreactivity, including cell body enlargement and shortened ramifications. Cognitive dysfunction following endotoxemia was also restored by pVNS.
Conclusion: Targeted cervical VNS using this novel percutaneous approach reduced LPS-induced systemic and brain inflammation and significantly improved cognitive responses. These results provide a novel therapeutic approach using bioelectronic medicine to modulate neuro-immune interactions that affect cognition.

Introduction

Dysregulated immunity is a major hallmark of several disease states and is an attractive target to treat or delay the onset of different conditions, including neurological disorders [1]. Neuroinflammation has been reported to be a critical driver of cognitive deficits, with glia cells playing a central role in this process [2]. Microglia, the resident immune cells of the central nervous system (CNS), continuously surveil the CNS microenvironment and rapidly respond to stimuli, adopting a reactive phenotype characterized by

Abbreviations: α7 nAChR, α7 subtype nicotinic acetylcholine receptors; BBB, blood-brain barrier; BCT, bradycardia threshold; ChAT, choline acetyltransferase; CNS, central nervous system; DG, dentate gyrus; DMX, dorsal motor nucleus of vagus; HR, heart-rate; Iba-1, ionized calcium binding adaptor molecule 1; LPS, lipopolysaccharide; NTS, nucleus tractus solitarius; PBS, phosphate buffer saline; pVNS, percutaneous vagus nerve stimulation; RT, room temperature; TNF-α, tumor necrosis factor-α.

* Corresponding author.
E-mail address: niccolo.terrando@duke.edu (N. Terrando).
[1] shared contribution.

https://doi.org/10.1016/j.brs.2018.10.005

enlarged cell bodies and shortened processes [3]. Although the role of microglial activation and the ensuing morphological changes remain unclear, these alterations are classically associated with pathological features following injury and infection [4]. Lipopolysaccharide (LPS), a key component of the outer membrane of gram-negative bacteria, is widely used to trigger neuroinflammation and ensuing behavioral changes, that are collectively termed "sickness behavior" [5]. Systemic endotoxemia induces pro-inflammatory cytokines and profound changes in microglial activity, followed by behavioral dysfunction and, in some cases, neurodegeneration [6].

The nervous system plays key roles in controlling immunity and fine-tuning responses to inflammatory challenges [7]. The identification of the "inflammatory reflex" provided the first description of a neural circuit capable of relaying information to the brain about the body's inflammatory status and modulating immunity *via* signaling through the vagus nerve [8]. Vagal signaling is crucial to the immune-regulatory and pro-resolving effects of this circuit [9]. Recently, electrical vagal nerve stimulation (VNS) was applied as an alternative therapy in patients with autoimmune disorders to inhibit tumor necrosis factor-α (TNF-α), one of the key inflammatory targets in rheumatoid arthritis [10]. The U.S. Food and Drug Administration has evaluated and approved VNS therapy for several conditions, including refractory epilepsy, depression, and migraine [11], although it remains unclear how these therapeutic effects are mediated.

VNS commonly requires surgical implantation of electrodes around the cervical vagus and has been reported both to attenuate systemic inflammation after LPS treatment [12] and reduce neuroinflammation in rodent models [13]. Although this approach provides direct nerve stimulation, the procedure is invasive and not amenable to acute or ambulatory settings. Non-invasive devices (i.e., transcutaneous VNS) have been developed with promising applications in humans thorough transauricular and transcervical approaches [14]. However, the specificity of these approaches and their ability to engage relevant target nerve fibers remain unclear. To overcome some of these limitations, we developed a novel approach to target selectively the vagus nerve in mice using ultrasound-guided needle electrode placement. This approach minimizes surgical manipulations, greatly improves the accuracy of vagal targeting, and can modulate ensuing inflammatory responses. We validated this model by assessing the vagal-dependent neural circuitry and evaluating the efficacy of this pVNS method in a model of endotoxemia with emphasis on microglia activation and cognitive function.

Material and methods

All animal procedures were approved by the Duke University Institutional Animal Care and Use Committee. Inbred male C57BL6/J mice, 12-weeks-old (stock #000664; Jackson Laboratories, Bar Harbor, ME), were housed 5 mice/cage under environmentally-controlled conditions on a 12 h/12 h light/dark cycle with *ad libitum* access to food and water. Mice were acclimated for at least 7 days before initiating any procedure. For behavioral testing, mice were transferred to the test rooms 18–24 h before testing and were maintained under the same environmental conditions as described above.

Percutaneous VNS (pVNS)

Mice were anesthetized with 6% sevoflurane (Sevotec Classic T3; SurgiVet, Norwell, MA) in an induction chamber and maintained under 3% sevoflurane *via* a nose-cone delivery system on a heated table. Body temperature was maintained at 37 °C and monitored using a rectal probe. Non-invasive pulse-oximetry was applied to the right paw to monitor heart rate in real-time (MouseSTAT Jr.; Kent Scientific Corporation, Torrington, CT). Mice were placed in a supine position and the fur on the ventral aspect of the neck area was removed using hair removal cream (Nair; Church & Dwight, Trenton NJ). A concentric-bipolar 26 G EMG needle electrode (TECA Elite Disposable Concentric Needle Electrode; Natus Neurology Incorporated, Madison, WI) was positioned superficially under the skin in the ventral area over the right cervical branch of the vagus nerve before applying ultrasound gel (Aquasonic 100, Parker Laboratories, Fairfield, NJ). The ultrasound transducer (VisualSonics Vevo 770 Ultrasound System, Toronto, ON, Canada) was placed in the transverse orientation and positioned to visualize the electrode and key anatomical landmarks in the neck area, including the carotid artery (by the pulsing movement and identification of blood flow using the Doppler function), trachea, and larynx (Fig. 1A). The needle electrode was then guided adjacent to the carotid sheath using a micromanipulator. The vagus was electrically stimulated using biphasic, charge-balanced pulses at 20 Hz with 300 μs pulse duration with sufficient amplitude to achieve a 10% reduction in heart-rate (HR), termed the bradycardia threshold (BCT). The vagal stimulation amplitude was reduced to 90% BCT for delivery of 30 min of stimulation (Pulsar 6bp-as; FHC, Bowdoin, ME) [15]

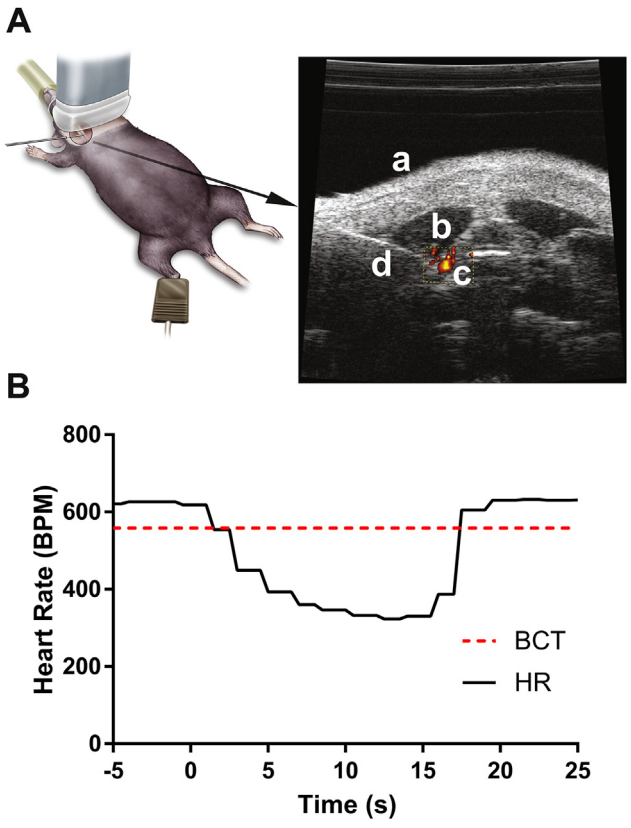

Fig. 1. Schematic representation of percutaneous method. **A)** Illustration of method. The animal is in supine position with the ultrasound transducer placed over the shaved cervical region. Anatomical landmarks used in needle positioning include: (a) ventral aspect of cervical region, (b) neck muscles, and (c) carotid artery with blood flow confirmed with Doppler imaging. Needle electrode (d) is visualized and the tip is positioned at the carotid sheath of the vagus for effective nerve stimulation (for a detailed view see **Suppl. Video**). **B)** Representative example of VNS-induced bradycardia. The period of stimulation is denoted with the black bar. Heart rate (HR) is markedly decreased with stimulation (time = 0 s) and quickly recovers (time = 15 s). Bradycardia is defined as a 10% reduction in HR and is plotted as the dashed line (BCT). Stimulation is applied as biphasic pulses at 20 Hz.

(**Suppl. Video**). A second stimulation paradigm was used in which BCT was identified at 20 Hz and, with the amplitude remaining constant, the frequency was decreased to 10 Hz for delivery of 30 min of stimulation. In both stimulation paradigms, bradycardia was induced for a short period (~10 s) before either *(1)* reducing amplitude to 90% BCT for 20 Hz stimulation or *(2)* reducing frequency to 10 Hz for 10 Hz stimulation, neither of which produced any bradycardic effects during the duration of the stimulation. Electrode placement without stimulation was performed in sham pVNS mice.

Supplementary video related to this article can be found at https://doi.org/10.1016/j.brs.2018.10.005.

Endotoxemia model

Lipopolysaccharide (LPS) derived from *Escherichia coli* endotoxin (0111:B4 ultra-pure; InvivoGen, San Diego, CA) was dissolved in 0.85% saline and mice were injected intraperitoneally with vehicle (controls) or with 1 mg/kg LPS in a 0.1 ml volume as described [16]. The vehicle or LPS was administered immediately after pVNS. Plasma and brain samples were collected at 3 and 24 h for cytokine expression and microglia activation studies, respectively. A separate cohort of mice underwent behavioral testing.

TNF-α ELISA

Plasma levels of TNF-α were evaluated at 3 h using a commercially available ELISA kit (BioSource, Camarillo, CA) *per* manufacturer's instructions. Blood was collected *via* thoracotomy under terminal anesthesia and centrifuged at 2000 g for 9 min at 4 °C, then stored at −80 °C before analysis.

Immunohistochemistry

Mice were deeply anesthetized with isoflurane and transcardially perfused using 20 ml of 0.1 M PBS (phosphate buffered saline) followed by 30 ml of 4% paraformaldehyde in 0.1 M PBS (pH 7.4). The brains were removed immediately and post-fixed for 3–4 days in 0.1 M PBS with 20% and then 30% sucrose at 4 °C. After post-fixation, 50 μm coronal sections from the brainstem region were obtained using a cryostat (Microm HM550; Thermo Scientific, Waltham, MA). Sections from naïve, sham, and pVNS treatment groups were processed in parallel. Separate sections were stained for c-Fos (goat anti-c-Fos, sc-52-G; Santa Cruz Biotechnology, Santa Cruz, CA), c-Fos/ChAT (rabbit anti-c-Fos, ab190289; Abcam, Cambridge, MA; goat anti-ChAT, AB144p; EMD Millipore, Burlington, MA) and Phospho-S6 ribosomal protein (Ser235/236) (rabbit anti-pospho S6, #2211; Cell Signaling Technologies, Danvers, MA). Sections were blocked with 10% normal donkey serum (D9663; Sigma-Aldrich, St. Louis, MO) and incubated for 48 h with primary antiserum. For single and double c-Fos/ChAT immunostaining, sections were incubated with primary antibodies (1:100) for 48 h at 4 °C. On the third day, the sections were washed in PBS and incubated in biotinylated secondary antiserum (against appropriate species IgG, 1:500 in PBS) for 2 h at room temperature (RT). The secondary antibodies used were: donkey anti-goat IgG (H+L) Cross-Adsorbed Secondary Antibody, Alexa Fluor 633; donkey anti-Rabbit IgG (H+L) Highly Cross-Adsorbed Secondary Antibody, Alexa Fluor 488 (all from Invitrogen, Carlsbad, CA). For staining of nuclei, DAPI (4′,6-Diamidino-2-phenylindole dihydrochloride, 1:1000; Sigma-Aldrich, St. Louis, MO) was applied for 20 min in PBS. The sections were mounted, dehydrated and cover-slipped. For negative controls, sections were incubated without the primary antibody to determine whether any non-specific staining was evident. Histology was performed by an investigator blinded to the experimental groups.

c-Fos and Phospho S6 quantification in the nucleus tractus solitarius (NTS) and the dorsal motor nucleus of the vagus nerve (DMX) was performed using 20X and 40X magnified images, respectively and counted bilaterally in 3 sections/brain, with sections taken across the rostral to caudal region of the NTS. Images were captured using a confocal laser scanning microscope (Leica TCS SP8). For counting c-Fos$^+$ and Phospho S6$^+$ cells, a semi-automatic analysis was used that was based upon threshold analysis, using the cell counter plugin of ImageJ software (Version: 1.51w). For quantification of co-localization of c-Fos and ChAT immunolabelling in the DMX, sections were subjected to threshold analysis at 40X magnification followed by a binary process where the signals were masked and merged to reveal the co-localized signal. The co-localized signals were counted using the cell counter plugin of ImageJ software. Counting was performed bilaterally and represented by mean counts per animal by an investigator blinded to the treatment conditions.

For analysis of microglia, the perfusion and staining methods described above were slightly modified. Tissues were post-fixed in 4% PFA for 24 h and sectioned at 75 μm using a vibratome (PELCO easiSlicer; Ted Pella, Inc., Redding, CA). Three hippocampal sections/brain were analyzed. Sections were incubated with rabbit anti-Iba1 (1:300; Wako Chemicals, Richmond, VA) and rat anti-CD68 (1:300; Bio-Rad) for 48 h at 4 °C followed by incubation with secondary antibodies for 2 h in RT. The secondary antibodies used were: donkey anti-rat IgG (H+L) Cross-Adsorbed Secondary Antibody, Alexa Fluor 488 antibody (1:500; Invitrogen) and donkey anti-rabbit Cy3 antibody (1:500; Jackson ImmunoResearch Inc.). Sections were DAPI stained and mounted. For quantification of morphological differences, images were captured at 40X magnification from the dentate gyrus (DG), CA1, and CA3 regions of the hippocampus. A z-stack of 20 μm–30 μm images was used for quantification from each experimental group. In each hippocampal subregion, two 40X images were taken. The images were subjected to threshold analysis using ImageJ software. A semi-quantitative analysis was performed by assigning values to microglia based upon the morphology observed. Based upon previously published work [17], values were assigned to each microglia based on changes in their soma and ramifications (thin soma and long processes vs. enlarged/elongated soma with thick processes) using the cell counter plugin function from ImageJ. The morphology counts for the experimental groups were the mean number of microglia morphologies from the total counts obtained per value (1 or 2) assigned to different morphological states of microglia. For Iba1/CD68 co-localization, z-stack images (63X, zoom 1 of z steps 0.75) were taken. The percent area of CD68 in Iba1$^+$ cells in the DG from 3 mice per group was measured using ImageJ as described in [18]. Histology was performed by an investigator blinded to the experimental groups.

Behavioral testing

Mice were behaviorally assessed under two different cognitive paradigms. Twenty-four h after LPS, or combined LPS + pVNS treatments, mice were acclimated for 5 min to a test arena (60 × 40 × 24 cm) designed to analyze the “what”, “where”, and “when” of memory as described [19]. The task was divided into three 5-min phases: exploration of set A objects, exploration of set B objects, and a final test phase with both A and B objects. A 50–55 min inter-trial interval was imposed between each phase. Following acclimatization, mice were exposed to four identical “A” objects presented in a triangular shape (3 objects near the “north” wall and the 4th object near the middle of the “south” wall). In

phase 2, mice were presented with four new identical "B" objects arranged in a square (each object near each corner). In the final phase, mice were tested using a new arrangement of objects. The "B" objects (termed "Recent B") remained in the "northeast" and "southwest" corners of the arena; an "A" object (termed "Stationary A") remained in the "northwest" corner; and a second "A" object (termed "Displaced A) was placed in the "southeast" corner. A video camera was mounted over the test area and was interfaced to a computer equipped with Noldus Ethovision 11.5 (Noldus Information Technology, Asheville, NC). Nose-point tracking recorded the duration of contacts with each object (i.e., nose within 2 cm of the object center and body axis of the mouse oriented towards the object). The duration of object investigation was determined for each test phase and preference scores were calculated for the "what", "where", and "when" memories with positive ratios denoting a specific memory and ratios approaching 0 signifying no evidence of this type of memory. "What" memory referred to the mean exploration time for both A objects minus that for the more recent B objects and divided by the total time investigating with both objects. "When" memory represented the difference between object interaction times for the "Stationary A" object and the mean times for both recent "B" objects, divided by the sum of those times. This distinguished old from recent memory. "Where" memory was calculated as the difference between object interaction times for the "Displaced A" object and the "Stationary A" object, divided by the total time with both objects. This metric reflected spatial memory.

Forty-eight h after LPS, or VNS + LPS treatments, memory load abilities were assessed as described [20]. Mice were subjected to seven different test trials, each separated by a 10–15 s inter-trial interval. In each trial, a new similarly sized object was added successively to the other objects in the arena (42 × 42 × 20 cm). For trials 1–3, mice were given 3 min each to explore objects. On trials 4–5 the exploration time was increased to 4 min and on trials 6–7 the mice were given 5 min to explore the objects. Testing began when the mouse was introduced into the arena with the first object. At the end of the trial the mouse was removed. If necessary, the arena was cleaned after mouse removal. The second object was added to the arena and the mouse was reintroduced to the arena. Mice were always placed initially in the same location relative to the objects. This procedure was repeated until all seven objects were presented. In each trial the newly added object was termed the "target" object. A video camera was mounted over the test arena and nose-point tracking was used as described above. The duration of time spent with the target object and the mean time spent with the remaining objects was calculated from the tracking profiles for each trial. Memory load was determined by the number of trials in which an animal successfully selected the new target object over the previously presented objects. Since memory load was sequentially defined over the consecutive trials, when a mouse no longer preferred the novel object the memory load of the mouse was considered full.

Statistics

The data are presented as mean ± SEM and were analyzed using GraphPad Prism (GraphPad v7.0 d; GraphPad Software, San Diego, CA) or SPSS 25 software (IBM, Armonk, NY). The data were analyzed by unpaired *t*-test, 2-WAY ANOVA, or repeated-measures ANOVA. *Post-hoc* analyses were by Bonferroni corrected pair-wise tests for the behavioral studies or Tukey's multiple comparison tests for the c-Fos analyses and microglial analyses. The CD68 datasets was analyzed by Kruskal–Wallis, followed by Dunn's multiple comparison tests. In all cases, statistical significance was set to $P < 0.05$.

Results

Effects of minimally invasive pVNS on brainstem nuclei activity

During ultrasound-guided needle electrode placement, pVNS was delivered to the right vagus nerve while mice were immobile under sevoflurane anesthesia (Fig. 1A, **Suppl. Video**). Bradycardia was assessed using non-invasive pulse oximetry to confirm effective stimulation of the vagus in real-time (Fig. 1B). No complications were observed following pVNS; however, one mouse was found dead within 24 h following LPS administration.

We quantified c-Fos immunoreactivity in the NTS 1 h after pVNS to confirm activation of vagal nerve fibers. The pVNS was observed to induce more c-Fos$^+$ immunostained cells in the ipsilateral NTS (120 ± 24; Fig. 2A and B) than either in the sham (38 ± 14) electrode placement but no stimulation) [$F(2, 8) = 17.36$, $P \leq 0.01$] or naïve controls (2 ± 2) [$F(2, 8) = 17.36$, $P = 0.001$]. No significant differences were found between naïve and sham groups. In the contralateral NTS, we found more c-Fos$^+$ cells after pVNS (69 ± 16) compared to sham (15 ± 5) [$F(2, 8) = 17.56$, $P \leq 0.01$] and the naïve group (0 ± 0) [$F(2,8) = 17.56$, $P \leq 0.01$]. Next, we assessed efferent fiber activation originating in the DMX. The number of c-Fos$^+$ immunoreactive cells increased after stimulation both in the ipsilateral (42 ± 9) and contralateral (27 ± 6) DMX as compared to the sham (9 ± 5 ipsilateral, 5 ± 3 contralateral) [$F(2, 8) = 17.18$, $P \leq 0.01$, and $F(2, 8) = 12.15$, $P \leq 0.05$] and naïve control groups (1 ± 1 ipsilateral, 1 ± 1 contralateral) [$F(2, 8) = 17.18$, $P \leq 0.01$, and $F(2,8) = 12.15$, $P \leq 0.01$ respectively] (Fig. 2C). It is noteworthy that there were no differences within groups in the numbers of c-Fos$^+$ cells between the ipsilateral and contralateral DMX nucleus at 1 h. A marker for cholinergic neurons is choline acetyltransferase (ChAT). This enzyme is expressed in the DMX and we quantified the effects of pVNS on cholinergic neuronal activity. The number of c-Fos/ChAT-double positive cells was increased in the DMX (30 ± 2 ipsilateral, 15 ± 1 contralateral) that received pVNS relative to the naïve controls (2 ± 1 ipsilateral, 2 ± 1 contralateral) [$F(2, 12) = 66.68$, $P \leq 0.001$] (Fig. 2D and E). The levels of c-Fos/ChAT activation were lower in the contralateral than ipsilateral DMX [$F(2, 12) = 9.642$, $P \leq 0.001$], while significantly more activation was still observed in the pVNS compared to naïve [$F(2, 12) = 66.68$, $P \leq 0.001$], but not sham mice (17 ± 2 ipsilateral, 7 ± 3 contralateral) [$F(2, 12) = 66.68$, $P = 0.01$]. In addition to c-Fos we also assessed ribosomal protein S6 phosphorylation as a marker to track neuronal activity [21]. pVNS treatment also resulted in increased levels of Phospho-S6 in the brainstem (337 ± 53) as compared to sham mice (68 ± 31, $P \leq 0.05$; Suppl. Fig. 1A and B).

Validation of pVNS on systemic inflammation after endotoxemia

We used a robust model of endotoxemia to test the efficacy of pVNS to modulate TNF-α, a stereotypical acute pro-inflammatory cytokine that is elevated 3 h after LPS administration, and its levels can be affected by surgical VNS [12]. We evaluated anti-inflammatory effects using two separate pVNS conditions at 10 Hz or 20 Hz stimulation. In the 10 Hz stimulation paradigm, the amplitude was maintained for 30 min at 100% of the BCT amplitude identified with 20 Hz test stimulation, and did not reduce the HR. In the second paradigm 20 Hz stimulation was maintained for 30 min at 90% of the BCT amplitude identified with 20 Hz test stimulation. LPS induced a robust elevation in plasma TNF-α at 3 h (617 ± 27.68 pg/ml) and this was reduced to similar extents by pre-emptive pVNS at 10 Hz (408.4 ± 20.62 pg/ml, $P \leq 0.001$) and 20 Hz (460.9 ± 37.45 pg/ml, $P = 0.007$; Fig. 3A); no significant differences were observed between the 10 and 20 Hz conditions.

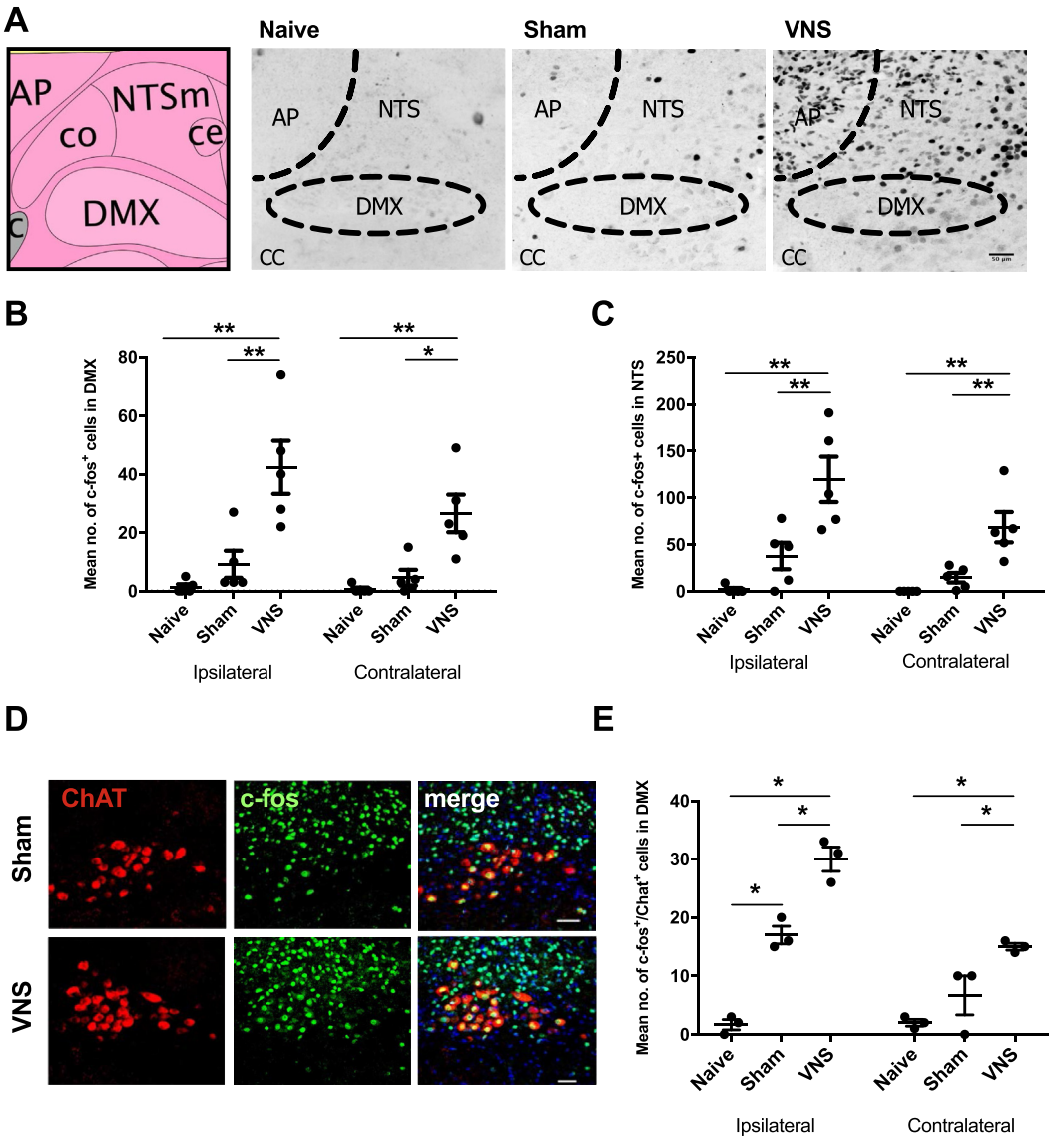

Fig. 2. c-Fos and ChAT activation in brainstem nuclei after pVNS. **A)** Schematic image from Allen Mouse Brain Atlas [http://mouse.brain-map.org/] illustrating the NTS and DMX region followed by representative images of c-Fos staining in naïve, sham, and 30 min pVNS mice. Images taken of brainstem region ipsilateral to stimulation after 20 Hz stimulation. Scale bar: 50 μm. **B)** Quantification of c-Fos$^+$ cells in the ipsilateral and contralateral NTS 1 h after pVNS. pVNS significantly induced c-Fos expression in the ipsilateral NTS. **C)** Quantification of c-Fos$^+$ cells in the ipsilateral and contralateral DMX 1 h after pVNS. Bilateral c-Fos$^+$ activation was detected after pVNS in the DMX. **D)** Representative images of ChAT (*left*) and c-Fos (*middle*) in the DMX (scale bar: 50 μm). Double-labeled neurons are visible in yellow (*right*) in the merged image. **E)** Quantification of ChAT$^+$/c-Fos$^+$ double-labeled cells following pVNS. Bilateral activation was evident in the DMX following 30 min pVNS. Abbreviations: nucleus tractus solitarius (NTS), dorsal motor nucleus of the vagus (DMX), area postrema (AP), central canal (CC), vagus nerve stimulation (VNS), choline acetyltransferase (ChAT). Data are presented as means ± SEMs and analyzed by two-way ANOVA and Tukey's *post-hoc* tests. N = 5 mice/group for panels B & C, and N = 3 for panel E $^*P < 0.05$, $^{**}P < 0.01$, $^{***}P < 0.001$, $^{****}P < 0.0001$ as indicated. (For interpretation of the references to colour in this figure legend, the reader is referred to the Web version of this article.)

Although in this study we used LPS to mimic a predictable challenge in the immune system, we sought to evaluate also the possible rescue properties of pVNS by injecting LPS prior to stimulation. Notably, 10 Hz stimulation significantly reduced TNF-α levels relative to the sham group (282.5 ± 20.68 pg/ml vs sham LPS group of 571.6 ± 56.31 pg/ml, $P \leq 0.001$; Fig. 3B) 3 h after LPS treatment (2.5 h after pVNS). However, no significant effect was observed with the 20 Hz stimulation condition (467.3 ± 55.52 pg/ml, $P = 0.200$).

Modulation of microglial morphology with pVNS

Next, we evaluated neuroinflammation by quantifying changes in microglial morphology 24 h after LPS administration and pVNS. Under physiological conditions microglia retain thin and ramified filopodia, critical to their surveillance function [22]. Following challenge, they modify their processes, enlarging their soma and retracting their ramifications, which are associated classically with changes in Iba-1 immunoreactivity. LPS induced morphological changes in microglia, and cells become non-ramified, their soma increased in volume, and there was retraction of their processes (Fig. 4A). Following pVNS at 10 Hz (17 ± 4) or 20 Hz (14 ± 7) fewer non-ramified microglia were observed compared to the LPS group (49 ± 8) [10 Hz: $F(2, 12) = 0.3649$, $P = 0.010$ and 20 Hz: $F(2, 12) = 0.8063$, $P = 0.009$]. Interestingly, more ramified cells were observed after 10 Hz pVNS (35 ± 8) relative to LPS-treated mice (5 ± 4, $P = 0.010$; Fig. 4B), whereas the 20 Hz pVNS group (23 ± 6) failed to reach significance. As anticipated, sham pVNS did not

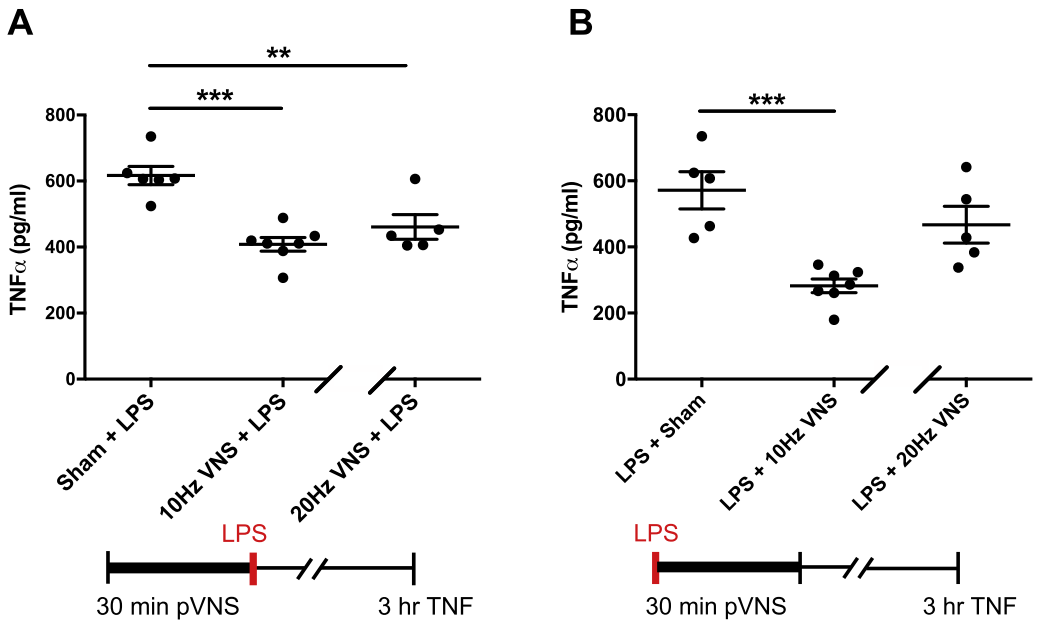

Fig. 3. Effects of pVNS on systemic TNF-α induction after endotoxemia. **A)** Preemptive pVNS, 10 or 20 Hz stimulation, significantly reduced LPS-induced TNF-α upregulation at 3 h (n = 5–7; ***P < 0.0001 and **P = 0.001 respectively). **B)** Rescuing effects of pVNS after LPS challenge. 10 Hz pVNS, but not 20 Hz stimulation, was able to reduce plasma TNF-α levels (n = 5–7; ***P < 0.0001). The data are presented as means ± SEMs and analyzed by *t*-tests. N = 5–7 mice/group.

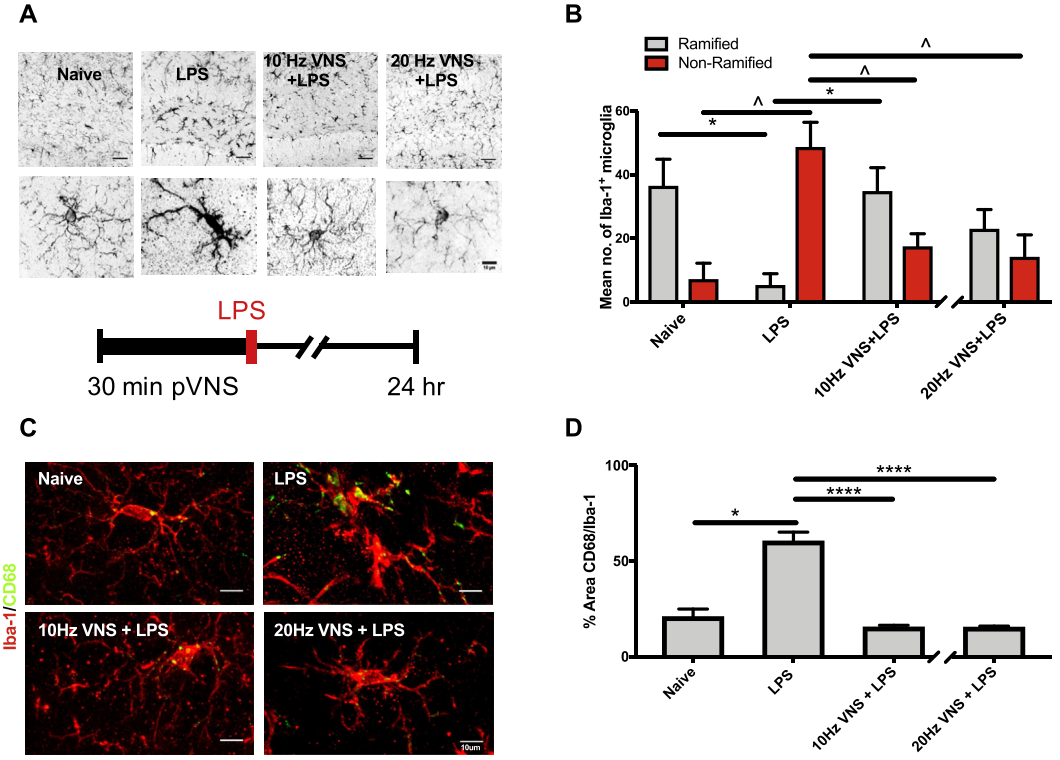

Fig. 4. Morphological changes in microglia following pVNS and LPS in hippocampus dentate gyrus region. **A)** Representative images of Iba-1 immunoreactivity in the DG in naïve, LPS (1 mg/kg), 10 and 20 Hz pVNS before LPS administration and representative segmented microglia cells from each of the experimental groups indicating the key morphological features quantified after pVNS and LPS treatments. Scale bars: 50 μm (*top panel*), 10 μm (*bottom panel*). **B)** Mean cell counts of ramified compared to non-ramified microglia. LPS induced significant changes in microglia morphology with a shift from ramified to non-ramified cells. Both 10 or 20 Hz pVNS reduced LPS-induced non-ramified microglial morphology. The 10 Hz pVNS restored ramified microglial morphology, but the 20 Hz stimulation was not significant. **C)** Representative images of Iba1$^+$/CD68$^+$ from the DG region across experimental groups. Scale bar: 10 μm. **D)** Quantification of the percent area of CD68 within Iba1$^+$ cells across experimental groups. The data are presented as means ± SEMs and were analyzed by two-way ANOVA and Tukey's *post-hoc* tests and for CD68% Area, Kruskal–Wallis, followed by Dunn's test. N = 3 mice/group, $^*P < 0.05$, $^{****}P < 0.0001$, LPS ramified vs. other ramified groups; $^{\wedge}P < 0.05$, LPS non-ramified vs. other non-ramified groups.

induce changes in microglial morphology as compared to naïve controls (36 ± 8 ramified, 7 ± 5 non-ramified, Suppl. Fig. 2A and B). Although these changes were more prominent in the hilus of the DG, similar alterations were observed also in the CA1 and CA3 hippocampus following pVNS treatment (Suppl. Fig. 2C-E). In addition to Iba-1 we also quantified the area occupied by the lysosomal marker CD68 in activated microglia (Fig. 4C). Increased CD68 immunoreactivity was observed 24 h after LPS (60.2 ± 4.9) compared to sham (13.0 ± 1.2, $P \leq 0.05$) and was significantly reduced by 10 (15.2 ± 1.2) and 20 Hz pVNS (15.1 ± 0.8, $P \leq 0.0001$ and $P \leq 0.0001$ respectively; Fig. 4D).

Rescue of memory deficits with pVNS

The "What-When-Where" task was used to examine three components of episodic memory; "what" was explored, "where" it was investigated, and "when" it was examined relative to adjacent events [19,23] (Suppl. Fig. 3A). To assess the relationship between neuroinflammation and cognitive functions, we evaluated the effects of pVNS on its ability to restore cognition in LPS-treated mice. We examined the responses of naïve mice, those treated with LPS, and those given 10 Hz or 20 Hz pVNS at the time of LPS administration. While the RMANOVA detected an overall trend among the different memory types [$F(2,60) = 1.506$, $P = 0.070$], the memory-types by treatment interaction was significant [$F(6,60) = 3.213$, $P = 0.008$] (Fig. 5A). Bonferroni corrected pair-wise comparisons were used to examine the responses within each type of episodic memory. In the "what" memory test, no significant differences were observed among the four groups. In the "when" test, LPS depressed object preference relative to the other three groups (Ps < 0.050). Interestingly, object preference was enhanced by the 10 ($P < 0.042$) and 20 Hz ($P < 0.023$) stimulation compared to the naïve group. In the "where" test, a similar relationship was observed where LPS depressed object preference relative to the other groups ($P = 0.003$). In this case, only the 10 Hz stimulation enhanced performance over that of the naïve control (Ps < 0.050). Together, the results indicate that "what" memory is unaffected by LPS or pVNS stimulation, whereby "when" and "where" memories benefitted from the pVNS, where the 10 Hz stimulation was particularly efficacious. Means and SEM for "What", "Where" and "When" Test are presented in Table 1.

Aside from episodic memory, mice were tested also for memory load [20]. Here, mice were evaluated for their ability to recognize a novel object when presented with the addition of a new to the already familiar objects over seven trials (Suppl. Fig. 3B). When exploration times for the novel object became indistinguishable among the other recently experienced objects, the memory load for the task was considered to be exceeded. A RMANOVA for within subject effects found significant main effects for the type of object (novel compared to average of other objects present in trial) [$F(1,36) = 127.009$, $P < 0.001$] and test-trial [$F(6,216) = 5.975$, $P < 0.001$]; the object type by treatment [$F(3,36) = 15.007$, $P < 0.001$], object type by trials [$F(6,18) = 15.954$, $P = 0.001$], and the three-way object type by test-trial by treatment [$F(18,216) = 1.612$, $P = 0.052$] interactions were also significant. Bonferroni corrected pair-wise comparisons revealed that within groups, the LPS and the 20 Hz + LPS animals failed to discriminate the novel from the familiar objects across the memory-load trials (Fig. 5B, *lower left and right*). By striking contrast, naïve mice spent significantly more time exploring the novel than familiar objects when the memory load was increased from 3 to 7 objects ($P \leq 0.003$) (Fig. 5B, *upper left*). Similarly, the 10 Hz + LPS group spent more time with the novel object when the memory load was augmented with 2 and 4–7 objects ($P \leq 0.041$) (Fig. 5B, *upper right*). Between groups on trial 1, the naïve mice spent more time with the novel object than LPS treated group ($P \leq 0.001$), whereas the 10 Hz+LPS and 20 Hz+LPS treatments were not distinguished from the naïve group or those animals given LPS alone. On trial 2, novel object exploration time was increased in the naïve relative to the LPS mice ($P = 0.020$). By trial 3, time with the novel object was enhanced in the sham compared to the LPS and the 20 Hz + LPS groups (Ps ≤ 0.033). The increased memory load on trials 4 and 5 found exploration of the novel object in the sham group to be higher than all other groups (Ps ≤ 0.054). On trial 6, novel object exploration time was augmented in the naïve and 10 Hz+LPS groups relative to the other mice ($P \leq 0.051$). Finally, when confronted with 7 objects, the sham mice spent more time with the novel object than all other groups ($P \leq 0.003$), while the 10 Hz+LPS group engaged the novel object more than the LPS and 20 Hz+LPS groups ($P \leq 0.017$). Together, these findings demonstrate that LPS impairs memory load beginning with the first pair of objects and that 20 Hz pVNS does not improve this condition. In contrast, naïve mice can recognize the novel object even when 7 objects are presented. The 10 Hz pVNS is efficacious in enabling this group to identify the novel object even in trials with as many as 6 familiar objects; however, their overall performance was not always equivalent to that of the naïve controls. Hence, the 10 Hz pVNS is highly efficacious and partial rescue is evident when memory load becomes high. Means and SEM for Memory Load Test are presented in Table 2.

Discussion

This study describes a novel minimally-invasive method to stimulate percutaneously the vagus nerve using ultrasound-guided needle electrode placement. Our results demonstrate that this new method, pVNS, modulates vagal activity and neuro-immune signaling as described with other VNS methods requiring surgical implantation of a cuff electrode around the nerve. Using a robust model of endotoxemia we describe the efficacy of this new approach to reduce systemic inflammation, modulate microglial activity in hippocampus, and to restore LPS-induced memory deficits in mice.

The vagus represents a prototypical immunoregulatory reflex circuit with an afferent projection able to sense inflammatory changes and an efferent projection that reduces production of pro-inflammatory cytokines [7]. Using pVNS of the right cervical branch of the vagus nerve we activated this circuitry as evidenced by higher c-Fos activity in the ipsilateral than contralateral NTS, where vagal afferent axons terminate [24]. Interestingly, we also describe bilateral c-Fos activation in the DMX, indicating that pVNS activates fibers in the right cervical vagus which leads to reflex-like activation of efferent fibers in both the ipsilateral and contralateral branches. Heightened activation of ipsilateral DMX neurons may also indicate antidromic activation of efferent fibers directly caused by stimulation. However, considering the combination of unilateral NTS and bilateral DMX c-Fos expression, the primary component of DMX activity is believed to be through reflex circuitry. DMX neurons strongly express ChAT [25], which is critically involved in the immune-regulatory "inflammatory reflex" [8]. pVNS increased the number of ChAT expressing neurons that also exhibited enhanced c-Fos immmuoreactivity in the ipsilateral DMX; thereby demonstrating that pVNS modulates not only cholinergic neurotransmission but also activation of the efferent anti-inflammatory pathway. It has been reported that VNS induces acetylcholine release *via* a subset of T lymphocytes that express ChAT, which suppress TNF-α production and downregulate pro-inflammatory genes [8]. Inhibition of this innate immune response requires the α7 subtype of the nicotinic acetylcholine receptor (α7 nAChR), which can be activated either by pharmacological agonists or direct electrical stimulation

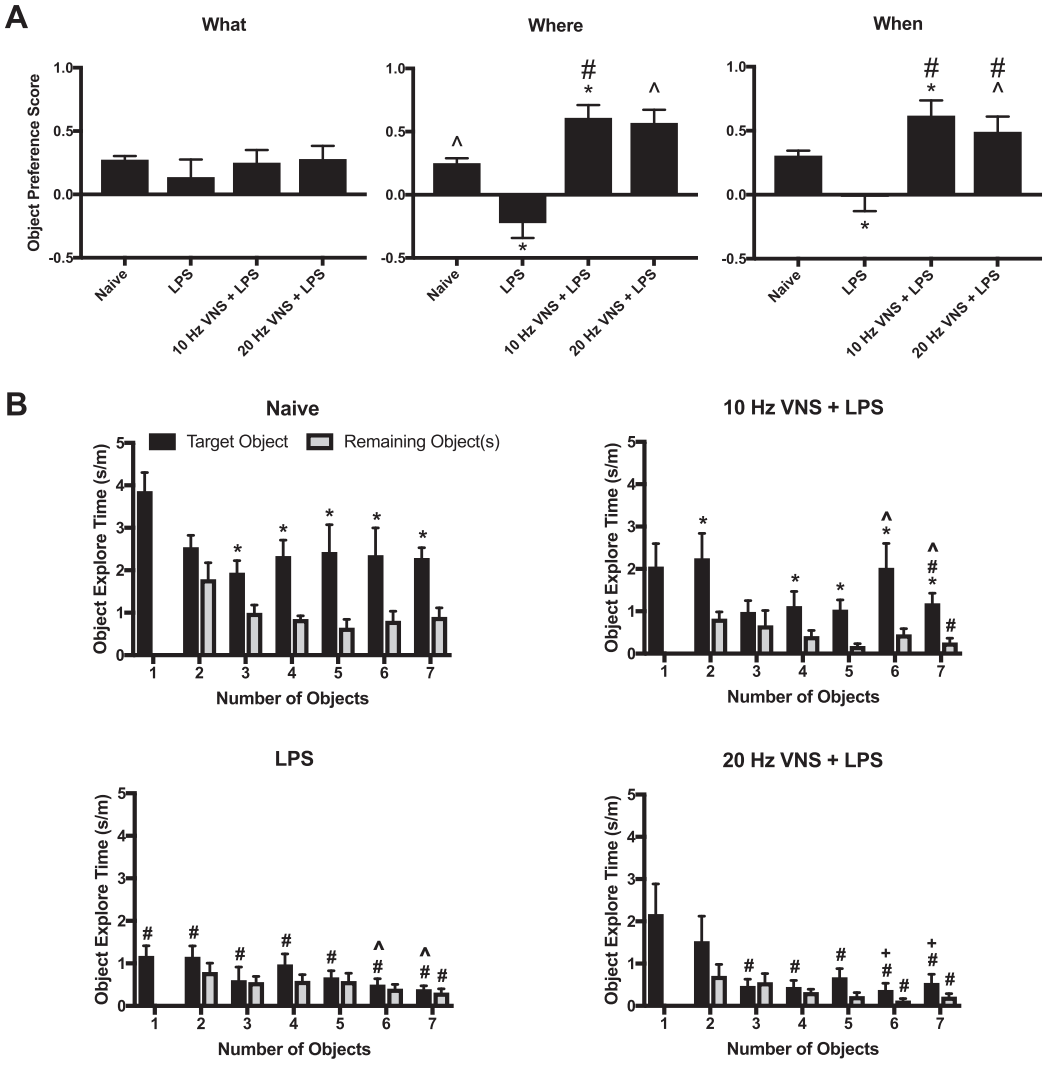

Fig. 5. pVNS rescues LPS-induced cognitive deficits. **A)** Object preference scores for the "What", "Where", and "When" memory task for naïve, 1 mg/kg (i.p.) LPS-t, 10 Hz + LPS-, and 20 Hz + LPS-treated mice. Animals were trained and tested 24 h after treatments. $^{\#}P < 0.05$, naïve vs other groups; $^{\wedge}P < 0.05$, LPS vs other groups. **B)** Object exploration times for the novel and now familiar objects in a memory load experiment that sequentially increased the numbers of total objects from 1 to 7 across the 7 consecutive trials. The same mice were used as in the previous episodic memory experiment, except they were tested at 48 h after treatments. The data are presented as means ± SEMs and analyzed by RMANOVA followed by Bonferroni corrected *post-hoc* tests. N = 16 mice in the LPS group and 8 mice each in the other three groups. $^{*}P < 0.05$, novel vs. other objects in a given trial; $^{\#}P < 0.05$, naïve vs other groups; $^{\wedge}P < 0.05$, LPS vs other groups; $^{+}P < 0.05$, between subjects effects vs. 10 Hz+LPS.

Table 1
Means and SEM for "What", "Where" and "When" test (Fig. 5A).

Treatment	n	"What" Memory		"Where" Memory		"When" Memory	
		Mean	SEM	Mean	SEM	Mean	SEM
Naive	8	0.271	0.032	0.247	0.041	0.301	0.042
LPS	16	0.092	0.095	−0.149	0.103	0.087	0.105
10 Hz VNS + LPS	8	0.246	0.104	0.605	0.104	0.614	0.122
20 Hz VNS + LPS	8	0.275	0.106	0.565	0.107	0.488	0.122

[12,24,26]. As pVNS enhanced ChAT/c-Fos double-positive immunoreactivity in the DMX, it suggests that this neuromodulatory effect is peripherally mediated. However, the key sites for this anti-inflammatory effect needs further elucidation and will be examined in future studies. In fact, while pVNS requires short periods eliciting bradycardia to ensure stimulation of the nerve, further work in pVNS may be able to reduce the need for such off-target effects while maintaining efficacy.

Systemic inflammation is associated with CNS dysfunction, including neuroinflammation and cognitive impairment [6]. Infection, including edotoxemia, rapidly elevates TNF-α which triggers a cascade of pro-inflammatory cytokines [16]. In our studies pVNS reduced systemic levels of TNF-α, a key cytokine that has been extensively studied in different pathologies. Pro-inflammatory cytokines can affect CNS functions and disrupt the blood-brain barrier (BBB). Interestingly, in a rat model of ischemic stroke, VNS decreased BBB disruption by reducing damage to tight junctions, endothelial cells, and astrocytes in the neurovascular unit [27]. LPS exerts variable effects on tight junctions and endothelial cells, depending upon the dosage and experimental models. Nevertheless, the deleterious effects on the BBB are strongly dependent on TNF-α release [28]. As noted in this study, pVNS reduced plasma levels of TNF-α both in prevention and rescue paradigms, suggesting that the systemic anti-inflammatory effects

Table 2
Means and SEM for memory load test (Fig. 5B).

Treatment	n	Number of Objects	Target Object (sec/m)		Remaining Objects (sec/m)	
			Mean	SEM	Mean	SEM
Naive	8	1 Object	3.85	0.44	–	–
		2 Objects	2.53	0.29	1.77	0.40
		3 Objects	1.92	0.29	0.98	0.19
		4 Objects	2.32	0.38	0.84	0.08
		5 Objects	2.41	0.65	0.63	0.20
		6 Objects	2.34	0.65	0.79	0.23
		7 Objects	2.27	0.25	0.89	0.22
LPS	16	1 Object	1.16	0.25	–	–
		2 Objects	1.14	0.26	0.78	0.21
		3 Objects	0.59	0.32	0.54	0.14
		4 Objects	0.96	0.25	0.57	0.15
		5 Objects	0.66	0.16	0.58	0.19
		6 Objects	0.48	0.15	0.38	0.11
		7 Objects	0.37	0.09	0.29	0.10
10 Hz VNS + LPS	8	1 Object	2.04	0.55	–	–
		2 Objects	2.23	0.60	0.81	0.16
		3 Objects	0.97	0.27	0.65	0.36
		4 Objects	1.11	0.35	0.40	0.14
		5 Objects	1.02	0.24	0.16	0.06
		6 Objects	2.01	0.58	0.44	0.14
		7 Objects	1.17	0.25	0.25	0.11
20 Hz VNS + LPS	8	1 Object	2.15	0.72	–	–
		2 Objects	1.51	0.60	0.69	0.28
		3 Objects	0.46	0.16	0.54	0.21
		4 Objects	0.43	0.16	0.31	0.07
		5 Objects	0.66	0.21	0.21	0.09
		6 Objects	0.36	0.17	0.11	0.05
		7 Objects	0.53	0.21	0.20	0.08

of pVNS may prevent secondary CNS damage and BBB disruption. Circulating macrophages, as well as resident microglia, express α7 nAChR [29]. Treatment with α7 nAChR agonists depress macrophage activity and inhibit TNF-α-induced NF-kB activation in bone marrow-derived macrophage cultures [30]. Cholinergic agonists can also affect microglial activation and improve cognitive outcomes after trauma and common perioperative complications, such as infection or stroke [31,32]. Although pharmacological agonists attenuate inflammation in several disease models, they exert off-target effects in other organs, which likely affect multiple physiologic processes ranging from gastrointestinal motility to wound healing [29,33–35]. VNS holds promise also for a more localized response and better patient-specific therapeutic outcomes with fewer side effects, especially through the implementation of targeted and minimally invasive approaches.

We used a robust paradigm with LPS (1 mg/kg) to induce neuroinflammation and changes in microglial morphology. Following endotoxemia, microglia lose their characteristic ramifications and become hypertrophic [36]. In our study pVNS improved microglial morphology after LPS injection, with more cells retaining ramified branches as found under homeostatic states. As anticipated, pVNS reduced microglial activation, including Iba-1 and CD68, at 24 h in a manner similar to other VNS approaches [13,37,38]. These effects on glia activation may result from the systemic anti-inflammatory effects of VNS leading to a reduction in the overall neuroinflammatory burden, including Toll-like receptors signaling, rather than through a direct action as mediated through α7 nAChRs on microglia cells. Notably, sex-specific differences in microglial activation have been described in mice following inflammatory challenges, including activation of Toll-like receptor 4 pathways [39,40], and in this study we focused on male mice. Future work will determine the mechanisms whereby VNS affects microglial morphology, including evaluation of sex differences, and how these changes may translate into improved microglial function.

Aside from microglia activation and inflammatory responses, we investigated whether pVNS could exert any effects on LPS-induced cognitive impairment using a variety of tests as has been reported by other investigators [41–43]. These studies focused upon two separate aspects of cognition – the “what”, “where”, and “when” of episodic memory and effects on memory load [19,20]. Interestingly, “what” memory was unaffected by all treatments. By contrast, “where” and “when” memories were adversely affected by LPS treatment. Both 10 Hz and 20 Hz pVNS prevented the LPS deleterious effects to become manifest during testing for the “where” and “when” tasks and, surprisingly, pVNS boosted performance on these tasks higher than that for the naïve control. In a further evaluation for cognitive efficacy, mice were subjected to a memory load test. The LPS treated mice were severely debilitated on this task as they were unable to identify the novel object in any of the 7 pairings. The 20 Hz pVNS failed to ameliorate this effect. By striking comparison, the 10 Hz pVNS group spent more time exploring the novel object when the memory load was increased from 2 or 4 to 7 objects. Moreover, the performance by this group was statistically indistinguishable from that of the sham mice with memory loads of 2, 3, and 6 objects. Thus, the 10 Hz pVNS was highly efficacious and partial rescue was fully evident even with a high memory load of 6 objects.

Prior VNS studies have marginally investigated how different stimulation parameters affect outcomes and efficacies. Yoo and colleagues [15] showed that 20 Hz stimulation of the right cervical branch of the vagus nerve reliably elicited bradycardia in dogs. We reproduced this finding in mice and demonstrated the utility of bradycardia as a biomarker for effective stimulation of the vagus nerve. We also wanted to identify a level of stimulation that could be associated with minimal, or no, cardiovascular effects. Since the HR response to VNS is both stimulation amplitude- and frequency-dependent, we manipulated these parameters in two ways. In the first case, the stimulation frequency was retained at 20 Hz while the amplitude was reduced to 90% BCT. In a second procedure, the stimulation frequency was reduced to 10 Hz and the amplitude remained constant at 100% BCT. In both paradigms, constant stimulation failed to produce sustained bradycardia (as previously defined as a 10% reduction in HR). Since the paradigms differed in both stimulation frequency and amplitude, it is not possible to identify the causes of the contrasting effects on immune responses and behavior. The neural circuitry that the VNS engages within the hippocampus and other brain areas remains poorly understood. Although the vagus nerve lacks direct anatomical projections to the hippocampus, VNS can modulate hippocampal function through multisynaptic networks [44]. These signaling pathways may be important for both neuronal plasticity [45] and cell proliferation in the dentate gyrus [46]. Notably, VNS can modulate synaptic plasticity in different ways, including enhancing long-term potentiation in the hippocampus, which can influence memory processing and behavior [47]. As the role of the vagus nerve in modulating cognition and inflammation becomes clearer, more effective stimulation parameters can be developed to modulate selectively these separate and integrated systems. Such approaches may include fully non-invasive methods, like high intensity focused ultrasound.

Conclusion

This study establishes a novel procedure for stimulating the vagus nerve using a minimally invasive percutaneous needle approach in mice. pVNS reduced systemic inflammation, counteracted changes in microglia morphology, and normalized to a certain extent the cognitive impairments following endotoxemia. Further studies are needed to define the mechanisms whereby VNS regulates its neuroprotective effects, including changes in microglia

activity, neuroinflammation, neuronal signaling, and behavior. Together, these results provide a novel therapeutic approach using bioelectronic medicine to modulate neuro-immune interactions and cognition.

Funding

The work was supported by the Duke Institute for Brain Sciences Incubator Award (2016–18), a School of Medicine voucher for studies conducted in the Mouse Behavioral and Neuroendocrine Analysis Core Facility (#1163), and by the National Institutes of Health R01 AG057525 and R21 AG055877-01A1 to NT.

Conflicts of interest

None.

Acknowledgements

We thank Dr. G. Allan Johnson, Ph.D. (Charles E. Putman University Professor of Radiology and Director of the Center for In Vivo Microscopy at Duke University) for providing access and assistance with the ultrasound setup and Christopher Means (Behavioral Core Facility at Duke University) for his diligent assistance in behavioral testing.

Appendix A. Supplementary data

Supplementary data to this article can be found online at https://doi.org/10.1016/j.brs.2018.10.005.

References

[1] Dalli J, Serhan CN. Immunoresolvents signaling molecules at intersection between the brain and immune system. Curr Opin Immunol 2017;50:48–54.
[2] Heneka MT, Carson MJ, El Khoury J, Landreth GE, Brosseron F, Feinstein DL, et al. Neuroinflammation in Alzheimer's disease. Lancet Neurol 2015;14(4):388–405.
[3] Davalos D, Grutzendler J, Yang G, Kim JV, Zuo Y, Jung S, et al. ATP mediates rapid microglial response to local brain injury in vivo. Nat Neurosci 2005;8(6):752–8.
[4] Colonna M, Butovsky O. Microglia function in the central nervous system during Health and neurodegeneration. Annu Rev Immunol 2017;35:441–68.
[5] Godbout JP, Chen J, Abraham J, Richwine AF, Berg BM, Kelley KW, et al. Exaggerated neuroinflammation and sickness behavior in aged mice following activation of the peripheral innate immune system. Faseb J 2005;19(10):1329–31.
[6] Hoogland IC, Houbolt C, van Westerloo DJ, van Gool WA, van de Beek D. Systemic inflammation and microglial activation: systematic review of animal experiments. J Neuroinflammation 2015;12:114.
[7] Pavlov VA, Tracey KJ. Neural regulation of immunity: molecular mechanisms and clinical translation. Nat Neurosci 2017;20(2):156–66.
[8] Rosas-Ballina M, Olofsson PS, Ochani M, Valdes-Ferrer SI, Levine YA, Reardon C, et al. Acetylcholine-synthesizing T cells relay neural signals in a vagus nerve circuit. Science 2011;334(6052):98–101.
[9] Mirakaj V, Dalli J, Granja T, Rosenberger P, Serhan CN. Vagus nerve controls resolution and pro-resolving mediators of inflammation. J Exp Med 2014;211(6):1037–48.
[10] Koopman FA, Chavan SS, Miljko S, Grazio S, Sokolovic S, Schuurman PR, et al. Vagus nerve stimulation inhibits cytokine production and attenuates disease severity in rheumatoid arthritis. Proc Natl Acad Sci U S A 2016;113(29):8284–9.
[11] Ben-Menachem E, Revesz D, Simon BJ, Silberstein S. Surgically implanted and non-invasive vagus nerve stimulation: a review of efficacy, safety and tolerability. Eur J Neurol 2015;22(9):1260–8.
[12] Borovikova LV, Ivanova S, Zhang M, Yang H, Botchkina GI, Watkins LR, et al. Vagus nerve stimulation attenuates the systemic inflammatory response to endotoxin. Nature 2000;405(6785):458–62.
[13] Meneses G, Bautista M, Florentino A, Diaz G, Acero G, Besedovsky H, et al. Electric stimulation of the vagus nerve reduced mouse neuroinflammation induced by lipopolysaccharide. J Inflamm (Lond) 2016;13:33.
[14] Yuan H, Silberstein SD. Vagus nerve and vagus nerve stimulation, a comprehensive review: Part II. Headache 2016;56(2):259–66.
[15] Yoo PB, Liu H, Hincapie JG, Ruble SB, Hamann JJ, Grill WM. Modulation of heart rate by temporally patterned vagus nerve stimulation in the anesthetized dog. Phys Rep 2016;4(2).
[16] Terrando N, Rei Fidalgo A, Vizcaychipi M, Cibelli M, Ma D, Monaco C, et al. The impact of IL-1 modulation on the development of lipopolysaccharide-induced cognitive dysfunction. Crit Care 2010;14(3):R88.
[17] Davis BM, Salinas-Navarro M, Cordeiro MF, Moons L, De Groef L. Characterizing microglia activation: a spatial statistics approach to maximize information extraction. Sci Rep 2017;7(1):1576.
[18] Cope EC, Briones BA, Brockett AT, Martinez S, Vigneron PA, Opendak M, et al. Immature neurons and radial glia, but not astrocytes or microglia, are altered in adult Cntnap2 and Shank3 mice, models of autism. eNeuro 2016;3(5).
[19] DeVito LM, Eichenbaum H. Distinct contributions of the hippocampus and medial prefrontal cortex to the "what-where-when" components of episodic-like memory in mice. Behav Brain Res 2010;215(2):318–25.
[20] Sannino S, Russo F, Torromino G, Pendolino V, Calabresi P, De Leonibus E. Role of the dorsal hippocampus in object memory load. Learn Mem 2012;19(5):211–8.
[21] Puighermanal E, Biever A, Pascoli V, Melser S, Pratlong M, Cutando L, et al. Ribosomal protein S6 phosphorylation is involved in novelty-induced locomotion, synaptic plasticity and mRNA translation. Front Mol Neurosci 2017;10:419.
[22] Ransohoff RM, El Khoury J. Microglia in Health and disease. Cold Spring Harb Perspect Biol 2015;8(1), a020560.
[23] Dere E, Huston JP, De Souza Silva MA. Integrated memory for objects, places, and temporal order: evidence for episodic-like memory in mice. Neurobiol Learn Mem 2005;84(3):214–21.
[24] Berthoud HR, Neuhuber WL. Functional and chemical anatomy of the afferent vagal system. Auton Neurosci 2000;85(1–3):1–17.
[25] Swanson LW, Simmons DM, Whiting PJ, Lindstrom J. Immunohistochemical localization of neuronal nicotinic receptors in the rodent central nervous system. J Neurosci 1987;7(10):3334–42.
[26] Wang H, Yu M, Ochani M, Amella CA, Tanovic M, Susarla S, et al. Nicotinic acetylcholine receptor alpha7 subunit is an essential regulator of inflammation. Nature 2003;421(6921):384–8.
[27] Yang Y, Yang LY, Orban L, Cuylear D, Thompson J, Simon B, et al. Non-invasive vagus nerve stimulation reduces blood-brain barrier disruption in a rat model of ischemic stroke. Brain Stimul 2018;11(4):689–98.
[28] Varatharaj A, Galea I. The blood-brain barrier in systemic inflammation. Brain Behav Immun 2017;60:1–12.
[29] de Jonge WJ, Ulloa L. The alpha7 nicotinic acetylcholine receptor as a pharmacological target for inflammation. Br J Pharmacol 2007;151(7):915–29.
[30] Terrando N, Eriksson LI, Ryu JK, Yang T, Monaco C, Feldmann M, et al. Resolving postoperative neuroinflammation and cognitive decline. Ann Neurol 2011;70(6):986–95.
[31] Terrando N, Yang T, Ryu JK, Newton PT, Monaco C, Feldmann M, et al. Stimulation of the alpha7 nicotinic acetylcholine receptor protects against neuroinflammation after tibia fracture and endotoxemia in mice. Mol Med 2015;20(1):667–75.
[32] Han Z, Li L, Wang L, Degos V, Maze M, Su H. Alpha-7 nicotinic acetylcholine receptor agonist treatment reduces neuroinflammation, oxidative stress, and brain injury in mice with ischemic stroke and bone fracture. J Neurochem 2014;131(4):498–508.
[33] Pinheiro NM, Santana FP, Almeida RR, Guerreiro M, Martins MA, Caperuto LC, et al. Acute lung injury is reduced by the alpha7nAChR agonist PNU-282987 through changes in the macrophage profile. Faseb J 2017;31(1):320–32.
[34] Li F, Chen Z, Pan Q, Fu S, Lin F, Ren H, et al. The protective effect of PNU-282987, a selective alpha7 nicotinic acetylcholine receptor agonist, on the hepatic ischemia-reperfusion injury is associated with the inhibition of high-mobility group box 1 protein expression and nuclear factor kappaB activation in mice. Shock 2013;39(2):197–203.
[35] Duris K, Manaenko A, Suzuki H, Rolland WB, Krafft PR, Zhang JH. alpha7 nicotinic acetylcholine receptor agonist PNU-282987 attenuates early brain injury in a perforation model of subarachnoid hemorrhage in rats. Stroke 2011;42(12):3530–6.
[36] Cardona AE, Pioro EP, Sasse ME, Kostenko V, Cardona SM, Dijkstra IM, et al. Control of microglial neurotoxicity by the fractalkine receptor. Nat Neurosci 2006;9(7):917–24.
[37] Farrand AQ, Helke KL, Gregory RA, Gooz M, Hinson VK, Boger HA. Vagus nerve stimulation improves locomotion and neuronal populations in a model of Parkinson's disease. Brain Stimul 2017;10(6):1045–54.
[38] Kaczmarczyk R, Tejera D, Simon BJ, Heneka MT. Microglia modulation through external vagus nerve stimulation in a murine model of Alzheimer's disease. J Neurochem;0(0).
[39] Sorge RE, LaCroix-Fralish ML, Tuttle AH, Sotocinal SG, Austin JS, Ritchie J, et al. Spinal cord Toll-like receptor 4 mediates inflammatory and neuropathic hypersensitivity in male but not female mice. J Neurosci 2011;31(43):15450–4.
[40] Doyle HH, Eidson LN, Sinkiewicz DM, Murphy AZ. Sex differences in microglia activity within the periaqueductal gray of the rat: a potential mechanism driving the dimorphic effects of morphine. J Neurosci 2017;37(12):3202–14.
[41] O'Connor JC, Lawson MA, Andre C, Moreau M, Lestage J, Castanon N, et al. Lipopolysaccharide-induced depressive-like behavior is mediated by indoleamine 2,3-dioxygenase activation in mice. Mol Psychiatr 2009;14(5):511–22.

[42] Sparkman NL, Kohman RA, Scott VJ, Boehm GW. Bacterial endotoxin-induced behavioral alterations in two variations of the Morris water maze. Physiol Behav 2005;86(1–2):244–51.
[43] Murray C, Sanderson DJ, Barkus C, Deacon RM, Rawlins JN, Bannerman DM, et al. Systemic inflammation induces acute working memory deficits in the primed brain: relevance for delirium. Neurobiol Aging 2012;33(3):603–616 e3.
[44] Castle M, Comoli E, Loewy AD. Autonomic brainstem nuclei are linked to the hippocampus. Neuroscience 2005;134(2):657–69.
[45] Biggio F, Gorini G, Utzeri C, Olla P, Marrosu F, Mocchetti I, et al. Chronic vagus nerve stimulation induces neuronal plasticity in the rat hippocampus. Int J Neuropsychopharmacol 2009;12(9):1209–21.
[46] Revesz D, Tjernstrom M, Ben-Menachem E, Thorlin T. Effects of vagus nerve stimulation on rat hippocampal progenitor proliferation. Exp Neurol 2008;214(2):259–65.
[47] Zuo Y, Smith DC, Jensen RA. Vagus nerve stimulation potentiates hippocampal LTP in freely-moving rats. Physiol Behav 2007;90(4):583–9.